Dynamic Behavior, Redistribution Reactions, and Intermetallic Distances of Dinuclear Bis(μ-pyrazolato)rhodium(I) Complexes

Cristina Tejel, José M. Villoro, Miguel A. Ciriano,* José A. López, Eduardo Eguizábal, Fernando J. Lahoz, Vladimir I. Bakhmutov, and Luis A. Oro*

Departamento de Química Inorgánica, Instituto de Ciencia de Materiales de Aragón, Universidad de Zaragoza-CSIC, E-50009 Zaragoza, Spain

Received January 3, 1996[⊗]

Replacement of the olefin in the complexes [{Rh(μ-RPz)(C_2H_4)$_2$}$_2$] (RPz = pyrazolate (Pz) (**1**), 3-methylpyrazolate (MePz) (**2**), 3,5-dimethylpyrazolate (Me_2Pz) (**3**)) by *tert*-butyl isocyanide gives [{Rh(μ-RPz)($CNBu^t$)$_2$}$_2$] (**4**, **5**, **6**) respectively. Complex **4** can alternatively be prepared from [{Rh(μ-Pz)(cod)}$_2$] (cod = 1,5-cyclooctadiene) (**7**) leading to a chemical equilibrium between **4**, **7**, and the intermediate [(cod)Rh(μ-Pz)$_2$Rh($CNBu^t$)$_2$] (**8**), which has been also isolated. Kinetic studies on this apparent ligand redistribution reaction, leading to **8**, show that it follows a second order rate, giving the activation parameters $\Delta H^{\neq} = 21.8$ kcal·mol^{-1}, $\Delta S^{\neq} = -7.4$ eu, and $\Delta G^{\neq 298} = 24.0$ kcal·mol^{-1}, suggesting that the dinuclear complexes are the active species, and no fragmentation seems to occur. The molecular structures of complexes **3**, **4**, **8**, and [{Rh(μ-Pz)(CO)$_2$}$_2$] (**9**) determined by X-ray diffraction show discrete dinuclear complexes with the six-membered "Rh(μ-Pz)$_2$Rh" ring showing a boatlike conformation. Complexes **3** and **4** present the shortest and the largest intermetallic nonbonding separations, 3.0961(2) and 3.8995(6) Å, respectively, so far reported in di-μ-pyrazolato-dirhodium(I) complexes. In addition, complex **3** shows the shortest olefinic C═C distance found in ethylene rhodium complexes and accordingly a very low activation energy, 10.0 kcal·mol^{-1}, for the rotation of the ethylene ligands. Complex **8** undergoes two independent intramolecular fluxional processes associated to the ring inversion of the six-membered "Rh(μ-Pz)$_2$Rh" metallacycle and to a σ-1,2-metallotropic shift showing activation parameters $\Delta H^{\neq} = 15.0$ kcal·mol^{-1}, $\Delta S^{\neq} = -1.7$ eu and $\Delta H^{\neq} = 19.7$ kcal·mol^{-1}, $\Delta S^{\neq} = 4.8$ eu, respectively. The first movement is influenced by medium effects and may be restricted by the ancillary ligands and the substituents on the pyrazolate rings in other bis(μ-pyrazolato) complexes. Finally, the intermetallic distance in dinuclear pyrazolato complexes is analyzed in terms of steric and electronic factors.

Introduction

The area of dimetallic complexes has aroused increased interest and great development in the field of organometallic chemistry. The central axis to this exploration has been the use of active metals such as rhodium or iridium together with binucleating ligands, in search of a compromise between the stability of the dimetallic complexes and their reactivity. Thus, pyrazolate ligands have been used due to their correct geometry to hold the two metal atoms in close proximity and the resulting flexibility of the dimetallic framework allowing the formation or breaking of metal−metal bonds.[1] These pyrazolato complexes and their related poly(pyrazolyl)borate compounds are under scrutiny,[2] providing new and interesting reactions such as C−H activation,[3] degradation of chlorocarbons,[4] and formation of hydroperoxo complexes[5] and alkoxycarbonyl complexes[6] as well as catalytic synergism.[7]

While an extensive study on the dinuclear bis(μ-pyrazolato)iridium(I) complexes (including oxidative-addition reactions,[8] kinetic,[9] electrochemistry,[10] photochemistry,[11] and theoretical studies[12]) has been carried

[⊗] Abstract published in *Advance ACS Abstracts,* May 15, 1996.

(1) (a) Usón, R.; Oro, L. A.; Ciriano, M. A.; Pinillos, M. T.; Tiripicchio, A.; Tiripicchio-Camellini, M. *J. Organomet. Chem.* **1981**, *205*, 247. (b) Usón, R.; Oro, L. A.; Ciriano, M. A.; Carmona, D.; Tiripicchio, A.; Tiripicchio-Camellini, M. *J. Organomet. Chem.* **1982**, *224*, 69. (c) Tiripicchio, A.; Lahoz, F. J.; Oro, L. A.; Pinillos, M. T. *J. Chem. Soc., Chem. Commun.* **1984**, 936. (d) Oro, L. A.; Pinillos, M. T.; Tiripicchio, A.; Tiripicchio-Camellini, M. *Inorg. Chim. Acta* **1985**, *99*, L13. (e) Pinillos, M. T.; Elduque, A.; Oro, L. A.; Lahoz, F. J.; Bonati, F.; Tiripicchio, A.; Tiripicchio-Camellini, M. *J. Chem. Soc., Dalton Trans.* **1990**, 989. (f) Balley, J. A.; Grundy, S. L.; Stobart, S. R. *Organometallics* **1990**, *9*, 536 and references therein. (g) Pinillos, M. T.; Elduque, A.; López, J. A.; Lahoz, F. J.; Oro, L. A. *J. Chem. Soc., Dalton Trans.* **1991**, 1391. (h) Carmona, D.; Ferrer, J.; Mendoza, A.; Lahoz, F. J.; Reyes, J.; Oro, L. A.; *Angew. Chem,. Int. Ed. Engl.* **1991**, *30*, 1171.

(2) Trofimenko, S. *Prog. Inorg. Chem.* **1986**, *34*, 115. Trofimenko, S. *Chem. Rev.* **1993**, *93*, 943.

(3) (a) Férnandez, M. J.; Rodriguez, M. J.; Oro, L. A.; Lahoz, F. J. *J. Chem. Soc., Dalton Trans.* **1989**, 2073. (b) Ghosh, K.; Graham, W. A. G. *J. Am. Chem. Soc.*, **1989**, *111*, 375. (c) Gutiérrez, E.; Monge, A.; Nicasio, M. C.; Poveda, M. L.; Carmona, E. *J. Am. Chem. Soc.* **1994**, *116*, 791.

(4) (a) Ciriano, M. A.; Tena, M. A.; Oro, L. A. *J. Chem. Soc., Dalton Trans.* **1992**, 2123. (b) Tejel, C.; Ciriano, M. A.; Oro, L. A.; Tiripicchio, A.; Tiripicchio-Camellini, M. *Organometallics* **1994**, *13*, 4153.

(5) Carmona, D.; Lamata, M. P.; Ferrer, J.; Modrego, J.; Perales, M.; Lahoz, F. J.; Atencio, R.; Oro, L. A. *J. Chem. Soc., Chem. Commun.* **1994**, 575.

(6) Carmona, D.; Ferrer, J.; Reyes, J.; Oro, L. A. *Organometallics* **1993**, *12*, 4241.

(7) Esteruelas, M. A.; García, M. P.; López, A. M.; Oro, L. A. *Organometallics* **1991**, *10*, 127.

(8) (a) Fjeldsted, D. O. K.; Stobart, S. R.; Zaworotko, M. J. *J. Am. Chem. Soc.* **1985**, *107*, 8258. (b) Bushnell, G. W.; Decker, M. J.; Eadie, D. T.; Stobart, S. R.; Vefghi, R. *Organometallics* **1985**, *4*, 2106 and references therein.

S0276-7333(96)00005-2 CCC: $12.00

out, the chemistry of the related (μ-pyrazolato)rhodium(I) complexes has been concentrated on substitution,[1a,b] some oxidative-addition,[1c,d,13] and hydroformylation reactions.[14] Both rhodium and iridium systems have π-acidic ancillary ligands, including diolefins, carbon monoxide, and tertiary phosphines. We are currently investigating the influence of markedly different ancillary ligands and/or substituted pyrazolates on the reactivity and properties of these systems. In this paper, we describe the synthesis of reactive pyrazolato−rhodium complexes with basic metal centers, some redistribution reactions involving dinuclear rhodium species along with a general study of the nonrigidity of dinuclear double bridged pyrazolato complexes, and an attempt to rationalize the variation of the intermetallic distance in these systems. Complex **4** has been previously reported in a preliminary communication.[4a]

Experimental Section

Starting Materials and Physical Methods. All reactions were carried out under argon using standard Schlenk techniques. [{Rh(μ-Cl)(cod)}$_2$],[15a] [{Rh(μ-Cl)(C_2H_4)$_2$}$_2$],[15b] and [{Rh(μ-RPz)(L$_2$)}$_2$] (RPz[1a] = Pz, L$_2$ = cod, (CO)$_2$; L$_2$ = cod, RPz = MePz,[15c] Me_2Pz[15d]) were prepared according to literature methods. All other chemicals were reagent grade and used without further purification. Solvents were purified according to standard procedures and distilled under argon prior to use. Carbon, hydrogen, and nitrogen analyses were performed using a Perkin-Elmer 2400 microanalyzer. IR spectra were recorded with a Perkin-Elmer 783 (4000−200 cm^{-1}) spectrophotometer with the infrared peaks of the complexes calibrated against the sharp peak (1601.4 cm^{-1}) of a polystyrene film. Mass spectra were recorded in a VG Autospec double-focusing mass spectrometer operating in the FAB$^+$ mode. Ions were produced with the standard Cs$^+$ gun at *ca.* 30 Kv, and 3-nitrobenzyl alcohol (NBA) was used as a matrix. ^{1}H, and ^{13}C{^{1}H} NMR spectra were recorded on Varian UNITY 300 and Bruker ARX 300 spectrometers operating at 299.95 and 300.13 MHz and at 75.42 and 75.47 MHz, respectively. Chemical shifts are reported in parts per million and referenced to Me_4Si using the signal of the deuterated solvent as reference. NMR probe temperatures were measured by a thermocouple calibrated with CD_3OD and ethylene glycol. Simulation of the dynamic behavior of complex **1** was carried out using the DNMR6 program[16] with the following parameters taken from the ^{1}H NMR static spectrum δ(A) = 2.476 ppm δ(B) = 2.690 ppm, δ(C) = 3.405 ppm, δ(D) = 3.666 ppm, and δ(Rh) = 100 000 ppm. J_{AB} = −0.19 Hz, J_{AC} = 14.99 Hz, J_{AD} = 10.07 Hz, J_{ARh} = J_{CRh} = 1.33 Hz, J_{BC} = 9.49 Hz, J_{BD} = 14.72 Hz, J_{BRh} = J_{DRh} = 1.55, and J_{CD} = 0.23 Hz. Thirteen ^{1}H NMR spectra of **1** in toluene-d_8 were recorded between 185 and 313 K and used in the simulation (correlation coefficient = 0.997). The variable temperature ^{1}H and ^{13}C{^{1}H} NMR spectra of complex **8** were recorded on deoxygenated samples at 10 different temperatures in toluene-d_8 (between 253 and 373K) and benzene-d_6 (between 283 and 333 K). The half-bandwidth for a given resonance is identical in both solvents at the same temperature.

Kinetic measurements for the formation of **8** have been carried out on two toluene-d_8 solutions containing equimolecular amounts of **4** and **7** (0.032 and 0.010 mol.L^{-1}) at seven temperatures between 323 and 358 K. Carefully deoxygenated samples were used; otherwise the results are irreproducible because the reaction is accelerated by oxygen. The variation of the concentration of the starting complexes in the mixtures were evaluated by the time-dependent integral intensities of the pyrazolate signals in the ^{1}H NMR spectra.

Preparation of the Complexes. [{Rh(μ-MePz)(C_2H_4)$_2$}$_2$] (**2**) and [{Rh(μ-Me_2Pz)(C_2H_4)$_2$}$_2$] (**3**) were prepared according to the general method described in ref 1a. Complex **2**. Yield: 77%. Anal. Calcd for $C_{16}H_{26}N_4Rh_2$: C, 40.02; H, 5.46; N, 11.67. Found: C, 39.92; H, 5.66; N, 11.55. Data for the major isomer follows: ^{1}H NMR (rt, $CDCl_3$) (δ, Hz): 7.23 (d, 1, 2H, H^{5}Pz); 5.76 (d, 1, 2H, H^{4}Pz); 3.25 (m, 16 H, HC=); 2.34 (s, 6H, MePz). ^{13}C {^{1}H} NMR (rt, $CDCl_3$) (δ, Hz): 145.9 (C^{3}Pz); 137.06 (C^{5}Pz); 104.1 (C^{4}Pz); 66.8 (d, J_{RhC} = 12 Hz, HC=); 66.6 (d, J_{RhC} = 11 Hz, HC=); 14.0 (*Me*Pz). MS (FAB$^+$, CH_2Cl_2, *m*/*z*, %): 480, 48% (M$^+$); 452, 100% (M − C_2H_4)$^+$; 424, 70% (M − 2C_2H_4)$^+$; 396, 47% (M − 3C_2H_4)$^+$; 368, 50% (M − 4C_2H_4)$^+$. Complex **3**. Yield: 93%. Anal. Calcd for $C_{18}H_{30}N_4Rh_2$: C, 42.54; H, 5.98; N, 11.03. Found: C, 42.18; H, 5.48; N, 11.05. ^{1}H NMR (rt, $CDCl_3$) (δ, Hz): 5.45 (s, 2H, H^{4}Pz); 3.34 (m, 16 H, HC=); 2.33 (s, 12 H, Me_2Pz). ^{13}C {^{1}H} NMR (rt, $CDCl_3$) (δ, Hz): 147.2 (C^{3,5}Pz); 103.8 (C^{4}Pz); 66.3 (d, J_{RhC} = 11 Hz, HC=); 14.0 (Me_2Pz).

[{Rh(μ-RPz)(CNBu^t)$_2$}$_2$] (RPz = Pz (4), 3-MePz (5), 3,5-Me_2Pz (6)). To a diethyl ether suspension (25 mL) of [{Rh(μ-RPz)(C_2H_4)$_2$}$_2$] (RPz = Pz (**1**), MePz (**2**), Me_2Pz (**3**)) (0.2 mmol) at about 5 °C in a ice bath was slowly added a stoichiometric amount of CNBu^t (89 μL, 0.4 mmol). The red or purple suspensions became yellow solutions in a few minutes (**5**, **6**) or gave a yellow microcrystalline precipitate (**4**). The resulting solutions or suspension were stirred for 2 h in the dark and concentrated to *ca.* 3 mL. A further addition of pentane (20 mL) rendered the products as microcrystalline yellow solids which were isolated by filtration under argon, washed with cold pentane, and dried in vacuo. These solids were stored under argon, in a refrigerator and in the dark. Complex **4** is also obtained and isolated in similar yield as described above but starting from [{Rh(μ-Pz)(cod)}$_2$] and adding 5 molar equiv of CNBu^t. Complex **4**. Yield: 95%. Anal. Calcd for $C_{26}H_{42}N_8Rh_2$: C, 46.44; H, 6.29; N, 16.66. Found: C, 46.52; H, 6.26; N, 16.57. IR (THF, cm^{-1}) ν(CN): 2135 (s), 2100 (s), 2060 (s). ^{1}H NMR (rt, benzene-d_6) (δ, Hz): 8.00 (d, 2, 4 H, H^{3,5}Pz); 6.47 (t, 2, 2 H, H^{4}Pz); 0.92 (s, 36H, CNBu^t). ^{13}C {^{1}H} NMR (rt, benzene-d_6) (δ, Hz): 151.9 (d, 56, *C*−Rh); 139.5 (C^{3,5}Pz); 102.6 (C^{4}Pz); 54.3 (*C*−(CH$_3$)$_3$); 29.6 (C−(*C*H$_3$)$_3$). MS (FAB$^+$, benzene, *m*/*z*, %): 672, 100% (M$^+$); 589, 10% (M − CNBu^t)$^+$. Complex **5**. Yield: 80%. Anal. Calcd for $C_{28}H_{46}N_8Rh_2$: C, 48.01; H, 6.62; N, 15.99. Found: C, 47.16; H, 6.35; N, 15.55. Data for the major isomer follows: ^{1}H NMR (rt, benzene-d_6) (δ, Hz): 7.83 (d, 1.6, 2H, H^{5}Pz); 6.26 (d, 1.6, 2H, H^{4}pz); 2.81 (s, 6H, MePz); 0.93 (s, 18 H, CNBu^t); 0.92 (s, 18 H, CNBu^t). ^{13}C {^{1}H} NMR (rt, benzene-d_6) (δ, Hz): 154.1 (d, 63,*C*−Rh); 151.8 (d, 63, *C*−Rh); 146.7 (C^{3}Pz); 141.1 (C^{5}Pz); 103.3 (C^{4}Pz); 55.3 (*C*−(CH$_3$)$_3$); 30.6 (C−(*C*H$_3$)$_3$); 16.0 (MePz). MS (FAB$^+$, benzene, *m*/*z*, %): 701, 100% (M$^+$); 617, 10% (M − CNBu^t)$^+$. Complex **6**. Yield: 77%. Anal. Calcd for $C_{30}H_{50}N_8Rh_2$: C, 49.45; H, 6.92; N, 15.38. Found: C, 48.76; H, 7.26;

(9) (a) Brost, R. D.; Stobart, S. R. *Inorg. Chem.* **1989**, *24*, 4308. (b) Brost, R. D.; Fjeldsted, D. O. K.; Stobart, S. R. *J. Chem. Soc., Chem. Commun.* **1989**, 488. (c) Brost, R. D.; Stobart, S. R. *Ibid.* **1989**, 498.
(10) Boyd, D. C.; Rodman, G. S.; Mann, K. R. *J. Am. Chem. Soc.* **1986**, *108*, 1779.
(11) (a) Marshall, J. L.; Hopkins, M. D.; Miskowski, V. M.; Gray, H. B. *Inorg. Chem.* **1992**, *31*, 5034. (b) Marshall, J. L.; Stobart, S. R.; Gray, H. B. *J. Am. Chem. Soc.*, **1984**, *106*, 3027.
(12) Lichtenberger, D. L.; Copenhaver, A. S.; Gray, H. B.; Marshall, J. L.; Hopkins, M. D. *Inorg. Chem.* **1988**, *27*, 4488.
(13) (a) Barceló, F.; Lahuerta, P.; Ubeda, M. A.; Foces-Foces, C.; Cano, F. H.; Martínez-Ripoll, M. *J. Chem. Soc., Chem. Commun.* **1985**, 43. (b) Powell, J.; Kuksis, A.; Nyburg, S. C.; Ng, W. W. *Inorg. Chim. Acta* **1982**, *64*, L211.
(14) (a) Kalck, Ph.; Thorez, A.; Pinillos, M. T.; Oro, L. A. *J. Mol. Catal.* **1985**, *31*,311 and references therein. (b) Claver, C.; Kalck, P.; Ridmy, M.; Thorez, A.; Oro, L. A.; Pinillos, M. T.; Apreda, M. C.; Cano, F. H.; Foces-Foces, C. *J. Chem. Soc., Dalton Trans.* **1988**, 1523.
(15) (a) Giordano, G; Crabtree, R. H. *Inorg. Synth.* **1979**, *19*, 218. (b) Cramer, R. *Inorg. Chem.* **1962**, *1*, 722. (c) Elguero, J.; Esteban, M.; Grenier-Loustalot, M. F.; Oro, L. A.; Pinillos, M. T. *J. Chim. Phys.* **1984**, *81*, 251. (d) Banditelli, G.; Bandini, A. L.; Bonati, F.; Minghetti, G. *J. Organomet. Chem.* **1981**, *218*, 229.
(16) Brown, J. H.; Bushweller, C. H. DNMR6: Calculation of NMR spectra (I = ½) Subject to the Effects of Chemical Exchange. QCPE Program No. 633, Indiana University.

Table 1. Crystallographic Data for 3, 4, 8, and 9

	[{Rh(μ-Me_2Pz)(C_2H_4)$_2$}$_2$] (**3**)	[{Rh(μ-Pz)($CNBu^t$)$_2$}$_2$] (**4**)	[(cod)Rh(μ-Pz)$_2$Rh($CNBu^t$)$_2$] (**8**)	[{Rh(μ-Pz)(CO)$_2$}$_2$] (**9**)
crystal color and habit	dark red, prismatic block	yellow, prismatic block	dark red, prismatic block	yellow-orange, irregular block
crystal size, mm	0.49 × 0.44 × 0.31	0.38 × 0.38 × 0.15	0.30 × 0.26 × 0.07	0.30 × 0.25 × 0.20
chem formula	$C_{18}H_{30}N_4Rh_2$	$C_{26}H_{42}N_8Rh_2$	C_{24} $H_{36}N_6Rh_2$	$C_{10}H_6N_4O_4Rh_2$
fw	508.28	672.50	614.41	452.01
temp, K	293(2)	233.0(2)	233.0(2)	293(2)
cryst syst	tetragonal	monoclinic	monoclinic	orthorhombic
space group	$P\bar{4}2_1m$ (No. 113)	$P2_1/c$ (No. 14)	$P2_1/c$ (No. 14)	*Pnma* (No. 62)
a, Å	11.1652(4)	11.3552(14)	17.367(3)	6.7455(6)
b, Å	11.1652(4)	11.2370(11)	9.993(2)	16.1596(13)
c, Å	8.0783(4)	25.185(4)	16.344(3)	12.9502(9)
β, deg	90.0	90.403(13)	97.760(10)	90.0
V, Å^3	1007.05(7)	3213.5(8)	2810.5(9)	1411.6(2)
Z	2	4	4	4
ρ(calcd), g cm^{-3}	1.68	1.39	1.45	2.13
μ, mm^{-1}	1.645	1.053	1.195	2.354
diffractometer	Siemens P4	Stoe-Siemens AED-2	Stoe-Siemens AED-2	Siemens P4
θ range data collecn, deg	2.5−30.8	1.6−25.0	2.4−25.0	2.0−29.2
index ranges	$-1 \le h \le 15$, $-1 \le k \le 16$, $-1 \le l \le 11$	$-13 \le h \le 0$, $-13 \le k \le 4$, $-29 \le l \le 29$	$-20 \le h \le 4$, $-11 \le k \le 0$, $-19 \le l \le 19$	$0 \le h \le 8$, $0 \le k \le 19$, $0 \le l \le 15$ $-8 \le h \le 0$, $-22 \le k \le 0$, $-15 \le l \le 0$
no. of collected reflcns	2508	8678	6661	3004
no. of unique reflcns	1121 (R_{int} = 0.0166)	5651 (R_{int} = 0.0192)	4926 (R_{int} = 0.0626)	1294 (R_{int} = 0.0162)
abs cor method	*ψ*-scan	*ψ*-scan	*ψ*-scan	*ψ*-scan
min., max. trans. factors	0.397, 0.494	0.692, 0.800	0.554, 0.690	0.396, 0.454
data/restraints/params	1120/0/78	5647/38/353	4924/52/289	1294/0/96
extinction coeff[a]	0.0194(9)	0.00065(13)		0.0169(4)
$R(F)$ [$F^2 > 2\sigma(F^2)$][b]	0.0148	0.0340	0.0565	0.0187
$R_w(F^2)$ (all data)[c]	0.0423	0.1011	0.1458	0.0411
S (all data)[d]	1.070	1.062	1.009	0.861

[a] See text. [b] $R(F) = \sum||F_o| - |F_c||/\sum|F_o|$, for 1106, 4726, 2527, and 800 observed reflections, respectively. [c] $R_w(F^2) = (\sum[w(F_o^2 - F_c^2)^2]/\sum[w(F_o^2)^2])^{1/2}$. [d] $S = [\sum[w(F_o^2 - F_c^2)^2]/(n - p)]^{1/2}$; n = number of reflections, p = number of parameters.

N, 14.85. IR (diethyl ether, cm^{-1}) *ν*(CN): 2133 (s), 2096 (s), 2052 (s). ^{1}H NMR (rt, benzene-d_6) (*δ*, Hz): 6.03 (s, 2H, H^{4}Pz); 2.77 (s, 12H, Me_2Pz); 0.95 (s, 36 H, $CNBu^t$). ^{13}C {^{1}H} NMR (rt, benzene-d_6) (*δ*, Hz): 153.0 (d, 64, *C*−Rh); 147.2 (C^{3,5}Pz); 103.0 (C^{4}Pz); 55.2 (*C*−(CH_3)$_3$); 30.6 (C−(*C*H_3)$_3$); 15.7 (*Me*$_2$Pz). MS (FAB$^+$, benzene, *m*/*z*, %): 729, 100% (M$^+$); 654, 30% (M − $CNBu^t$)$^+$.

[(cod)Rh(μ-Pz)$_2$Rh($CNBu^t$)$_2$] (8). To a solution of [{Rh(μ-Pz)(cod)}$_2$] (500 mg, 0.9 mmol) in THF (60 mL) was added a solution of $CNBu^t$ (200 μL, 1.8 mmol) in THF (40 mL) dropwise for 45 min. The resulting orange solution was stirred for 30 min and the solvent evaporated to dryness under vacuum. The extraction of the residue with cold pentane (2 × 20 mL) and subsequent filtration through anhydrous $MgSO_4$ gave an orange solution from which complex **8** was crystallized by evaporation to the pentane to *ca*. 3 mL. A second crop of crystals was obtained by refluxing the insoluble residue in pentane (mostly containing [{Rh(μ-Pz)(cod)}$_2$] and [{Rh(μ-Pz)($CNBu^t$)$_2$}$_2$]) and then in toluene for 3 h and further evaporation to dryness and extracting with pentane as described above. The overal yield is 55%. Anal. Calcd for $C_{24}H_{36}N_6Rh_2$: C, 46.91; H, 5.92; N, 13.68. Found: C, 47.08; H, 5.90; N, 13.55. IR (pentane, cm^{-1}) *ν*(CN): 2138 (s), 2062 (s). ^{1}H NMR (−20 °C, toluene-d_8) (*δ*, Hz): 7.87 (d, 1.7, 2 H, H^{3}Pz); 7.50 (d, 1.7, 2 H, H^{5}Pz); 6.34 (t, 1.7, 2 H, H^{4}Pz); 4.29 (m, 2 H, HC═); 4.16 (m, 2 H, HC═); 2.71 (m,2 H, H_2C^{exo}); 2.50 (m, 2 H, H_2C^{exo}); 1.79 (m, 4 H, H_2C^{endo}); 0.90 (s, 36 H, $CNBu^t$). ^{13}C {^{1}H} NMR (−20 °C, toluene-d_8) (*δ*, Hz): 151.5 (d, 64, *C*−Rh); 140.2 and 137.3 (C^{3,5}Pz); 104.7 (C^{4}Pz); 80.4 (d, 13, HC═) and 79.7 (d, 11, HC═); 55.8 (*C*−(CH_3)$_3$); 31.9 and 31.6 (H_2C); 30.5 (C−(*C*H_3)$_3$). MS (FAB$^+$, benzene, *m*/*z*, %): 614, 100% (M$^+$); 531, 4% (M − $CNBu^t$)$^+$.

X-ray Structural Analyzes of Complexes [{Rh(μ-Me_2Pz)(C_2H_4)$_2$}$_2$] (3), [{Rh(μ-Pz)($CNBu^t$)$_2$}$_2$] (4), [(cod)Rh(μ-Pz)$_2$Rh($CNBu^t$)$_2$] (8), and [{Rh(μ-Pz)(CO)$_2$}$_2$] (9). A summary of crystal data and refinement parameters is reported in Table 1. Crystals suitable for the X-ray diffraction studies were obtained in all cases from a pentane solution. Data were collected on a Stoe-Siemens AED-2 or on Siemens P4 diffractometers, with graphite-monochromated Mo Kα radiation using the *ω*/2*θ* scan method (*λ*(Mo Kα) = 0.710 73 Å). Three standard reflections were monitored every 55 min of measured time (**4**, **8**) or every 97 measured reflections (**3**, **9**) throughout data collection; no relevant variations were observed. All data were corrected for absorption using a semi-empirical method (*ψ*-scan)[17]; minimum and maximum transmission factors are listed in Table 1. All structures were solved by direct methods (SIR92)[18] and conventional Fourier techniques, and refined by full-matrix least-squares methods on F^2 (SHELXL-93).[19] Anisotropic thermal parameters were used in the last cycles of refinement for all non-hydrogen atoms, excepting those atoms involved in static disorders (**4** and **8**). The function minimized was $\sum[w(F_o^2 - F_c^2)^2]$ with the weighting scheme defined as $w^{-1} = [\sigma^2(F_o^2) + (xP)^2 + yP]$ ($P = (F_o^2 + 2F_c^2)/3$). For three structures an empirical extinction correction was applied, using the formula $F_c^* = F_c k[1 + 0.001x\ F_c^2\ \lambda^3/(\sin 2\theta)]^{-1/4}$, where *x* is the refined coefficient. Atomic scattering factors, corrected for anomalous dispersion, were used as implemented in the refinement program.[19]

Data for 3. A dark red prismatic block was indexed to tetragonal symmetry. All hydrogen atoms were localized in difference Fourier maps. Those bonded to the pyrazolate ligands were refined as free isotropic atoms while the remaining were fixed riding on their respective carbon atoms with free isotropic displacement parameters. The refinement converged to $R(F) = 0.0148$ and $R_w(F^2) = 0.0423$, with weighting parameters $x = 0.0244$ and $y = 0.0638$. Largest peak and hole in the difference map were +0.31 and −0.30 e Å^{-3}. The Flack parameter refined to −0.05(4), an indication of the correct determination of the crystalline absolute structure.

(17) North, A. C. T.; Phillips, D. C.; Mathews, F. S. *Acta Crystallogr., Sect. A* **1968**, *24*, 351.
(18) Altomare, A.; Cascarano, G.; Giacovazzo, C.; Guagliardi, A. *J. Appl. Crystallogr.* **1994**, *27*, 435.
(19) Sheldrick, G. M. *SHELXL-93*; University of Göttingen: Göttingen, Germany, 1993.

Data for 4. A yellow prismatic block was mounted and indexed to monoclinic symmetry. The *tert*-butyl groups of two terminal $CNBu^t$ ligands were observed disordered. They were modeled with three different positions for each methyl group, with restrained geometry. The occupancy factors were refined but fixed complementary to 1.0 (0.38(2), 0.34(2), 0.28(2) and 0.43(2), 0.43(2), 0.14(2)). The hydrogen atoms were included in calculated positions and refined riding on their carbon atoms with two common thermal parameters. The refinement converged to $R(F) = 0.0340$ and $R_w(F^2) = 0.1011$, with weighting parameters $x = 0.0517$ and $y = 4.9326$. Residual peaks in the final difference map were +0.79 and −0.38 e Å^{-3}.

Data for 8. A dark-red prismatic block was used and indexed to monoclinic symmetry. The *tert*-butyl groups of the $CNBu^t$ ligands were observed disordered. They were modeled with two different positions for each methyl group, with restrained geometry. The occupancy factors were refined but fixed complementary to 1.0 (0.57(3), 0.43(3) and 0.52(3), 0.48(3)). The hydrogens of the carbon atoms bonded to the metals were located in the difference Fourier maps, but the remaining hydrogens not involved in disorder were included in calculated positions. All of them were refined riding on their respective carbon atoms with two common thermal parameters. The refinement converged to $R(F) = 0.0565$ and $R_w(F^2) = 0.1458$, with weighting parameters $x = 0.0618$ and $y = 2.0422$. Largest peak and hole in the final difference map were +0.74 and −0.51 e Å^{-3}.

Data for 9. A yellow-orange irregular block was mounted and indexed to orthorhombic symmetry. The hydrogen atoms were localized in difference Fourier maps and were refined riding on their carbon atoms with a common isotropic displacement parameter. The refinement converged to $R(F) = 0.0187$ and $R_w(F^2) = 0.0411$, with weighting parameters $x = 0.0213$ and $y = 0$. Largest peak and hole in the difference map 0.32 and −0.35 e Å^{-3}.

Results

Synthesis of the Complexes. Redistribution Reactions. Reaction of the compounds $[\{Rh(\mu\text{-RPz})(C_2H_4)_2\}_2]$ (RPz = pyrazolate (Pz) (**1**), 3-methylpyrazolate (MePz) (**2**), 3,5-dimethylpyrazolate (Me_2Pz) (**3**)) with *tert*-butyl isocyanide ($CNBu^t$) under mild conditions gives the complexes $[\{Rh(\mu\text{-RPz})(CNBu^t)_2\}_2]$ (RPz = Pz (**4**), MePz (**5**), Me_2Pz (**6**)) in high isolated yields. Complex **4** can be also prepared by replacement of 1,5-cyclooctadiene (cod) in $[\{Rh(\mu\text{-Pz})(cod)\}_2]$ (**7**) by $CNBu^t$ (1:5 molar ratio) in an inert solvent such as diethyl ether. The complexes are yellow, air and moisture sensitive crystalline solids and were characterized by analytical and spectroscopic methods and by a single-crystal X-ray diffraction analysis for complex **4** (Figure 1). According to the ^1H and $^{13}C\{^1H\}$ NMR spectra of **4**−**6**, the boat conformation of the central Rh_2N_4 ring observed in the solid state (vide infra) is maintained in solution. Thus, the $^{13}C\{^1H\}$ NMR spectra for **4** and **6** show equivalent pyrazolate and isocyanide ligands while the isocyanide carbon bonded to rhodium gives rise to a doublet through coupling with the active ^{103}Rh nucleus. For the MePz derivative (**5**), the two diastereoisomers arising from the relative head-to-head (HH) and head-to-tail (HT) disposition of the bridging ligands are present in a 1:1.7 molar ratio respectively in solution. Mass spectra of complexes **4**−**6** are as expected for the dinuclear formulation.

Monitoring these reactions by ^1H NMR shows the replacement of cod is gradual while that of ethylene is non-selective. For example, a mixture of **4**, **7**, and $[(cod)Rh(\mu\text{-Pz})_2Rh(CNBu^t)_2]$ (**8**) in a 6:3:1 molar ratio is observed after the addition of 3 equiv of $CNBu^t$ to **7**. Subsequent heating of this mixture at 60 °C reveals the variation of the relative proportions of the three compounds, which leads to an enrichment of **8** and the detection of a fluxional behavior for this complex (see below). The former suggests the following redistribution reaction:

$$[\{Rh(\mu\text{-Pz})(cod)\}_2] + [\{Rh(\mu\text{-Pz})(CNBu^t)_2\}_2] \rightleftarrows 2[(cod)Rh(\mu\text{-Pz})_2Rh(CNBu^t)_2]$$

This equilibrium can be observed by monitoring the evolution of an equimolecular mixture of $[\{Rh(\mu\text{-Pz})(cod)\}_2]$ and $[\{Rh(\mu\text{-Pz})(CNBu^t)_2\}_2]$ in toluene-d_8 using ^1H NMR. Although it proceeds very slowly at room temperature, on heating the reaction mixture at 90 °C for 2 h., the molar fraction of **8** increases as far as 0.5. Conversely, solutions of **8** decompose slowly at room temperature, giving **4** and **7**, but this reaction can be quenched at −20 °C. From enriched solutions of **8**, the compound can be isolated in moderate yield as an air and moisture sensitive reddish-yellow solid, which has been characterized by X-ray diffraction (Figure 2). The solid-state molecular structure is retained in solution as shown by the ^1H and $^{13}C\{^1H\}$ NMR spectra in the slow-exchange region, where three resonances for the equivalent pyrazolate ligands and two for the olefinic protons and carbons are observed.

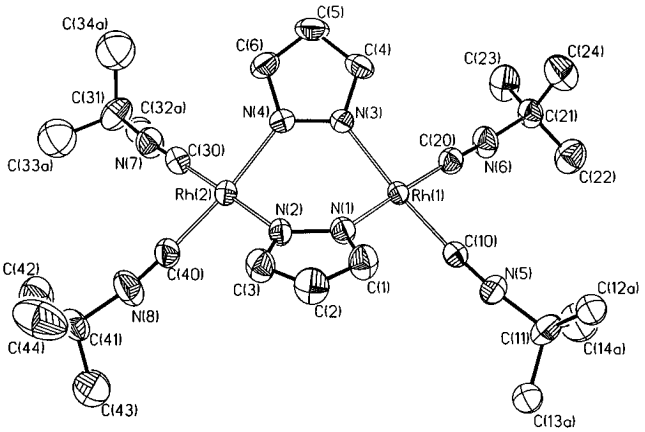

Figure 1. Molecular diagram of the $[\{Rh(\mu\text{-Pz})(CNBu^t)_2\}_2]$ (**4**) complex.

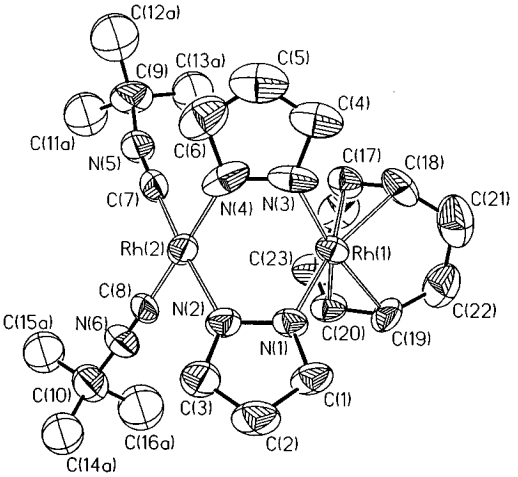

Figure 2. Molecular diagram of the $[(cod)Rh(\mu\text{-Pz})_2Rh(CNBu^t)_2]$ (**8**) complex.

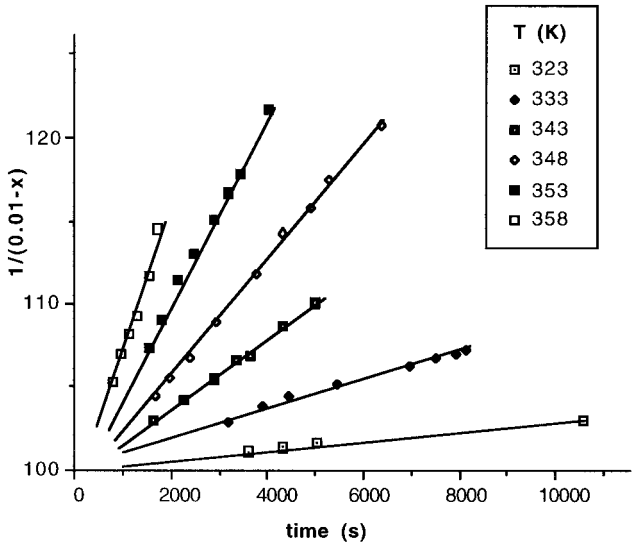

Figure 3. Kinetic plots for the reaction **4** + **7** ⇌ **8** at several temperatures. (0.01− *x*) represents the current concentration of **4** or **7**.

Kinetic measurements for the formation of **8** have been carried out on two toluene-d_8 solutions containing equimolecular amounts of **4** and **7** (0.032 and 0.010 mol/L). The data obtained have been treated in terms of a second-order reaction and the rate constants, *k*, calculated from these measurements. This gave a constant value for *k*. The results of the variable-temperature kinetic experiments (Figure 3) allow the calculation of the activation parameters $\Delta H^{\neq} = 21.8$ kcal·mol^{-1}, $\Delta S^{\neq} = -7.4$ eu and $\Delta G^{\neq 298} = 24.0$ kcal·mol^{-1}. It should be noted that the negative $\Delta S^{\neq}$ magnitude corresponds to the bimolecular character of the studied reaction.

We have tested that redistribution equilibria similar to the above described occur between other pyrazolate complexes with different ancillary and bridging bridges.

Molecular Structures of [{Rh(μ-Me$_2$Pz)(C$_2$H$_4$)$_2$}$_2$] (3), [{Rh(μ-Pz)(CNBu^t)$_2$}$_2$] (4), [(cod)Rh(μ-Pz)$_2$Rh(CNBu^t)$_2$] (8), and [{Rh(μ-Pz)(CO)$_2$}$_2$] (9). In order to structurally characterise the dinuclear bis(μ-pyrazolato)dirhodium(I) complexes the crystal structures of the new complexes **3**, **4**, and **8**, and the related tetracarbonyl derivative **9** were carried out. Their respective molecular structures are presented in Figures 4, 1, 2 and 5, together with the atomic labeling schemes used. Selected bond distances and angles are collected in Tables 2−5.

In each case the two pyrazolates, or substituted pyrazolate ligands (**3**), link the two metal centers, with intermetallic separations in the range 3.0961(2)−3.8996(6) Å (see Table 6). Interestingly, complexes **3** and **4** are at the extremes of this range. These complexes represent the shortest and the largest intermetallic separations so far reported in bis(μ-pyrazolato)dirhodium(I) complexes without invoking the presence of a metal−metal bond.[20] Each rhodium atom completes a distorted square-planar coordination sphere with two additional ligands; two ethylene molecules (**3**), two *tert*-butyl isocyanide ligands (**4**), two CNBu^t groups or a cod molecule (**8**), and two carbonyls (**9**). The main structural feature which characterises each of the complexes, is the boatlike conformation of the "Rh$_2$N$_4$" six-membered metallacycle. This is consistent for all cases where two pyrazolate ligands bridge two formally d^8

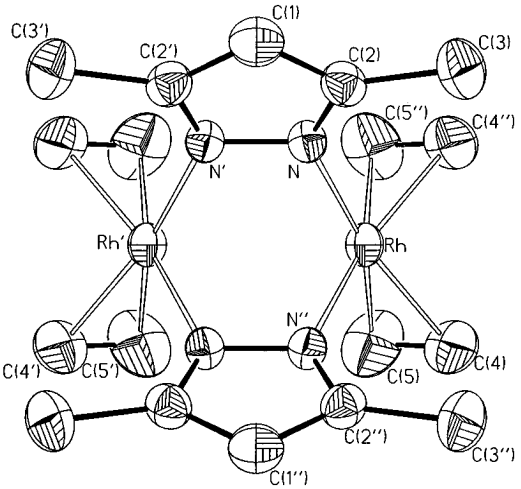

Figure 4. Molecular diagram of the [{Rh(μ-Me$_2$Pz)(C$_2$H$_4$)$_2$}$_2$] (**3**) complex. Primed atoms are related to the unprimed ones by the symmetry transformations $^1/_2 + y$, $-^1/_2 + x$, *z* (primed) and $^1/_2 - y$, $^1/_2 - x$, *z* (doubly primed).

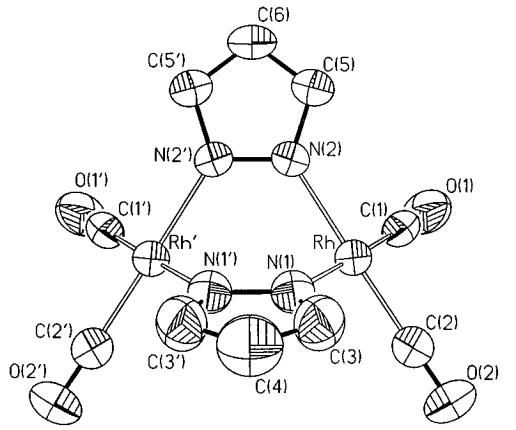

Figure 5. Molecular diagram of the [{Rh(μ-Pz)(CO)$_2$}$_2$] (**9**) complex. Primed atoms are related to the unprimed ones by the symmetry transformation *x*, $^1/_2 - y$, *z*.

Table 2. Bond Lengths (Å) and Selected Angles (deg) for 3[a]

Rh···Rh′	3.0961(2)	N−N′	1.374(3)
Rh−N	2.083(2)	N−C(2)	1.344(2)
Rh−C(4)	2.151(3)	C(1)−C(2)	1.388(2)
Rh−C(5)	2.147(4)	C(2)−C(3)	1.497(3)
Rh−M	2.042(4)	C(4)−C(5)	1.335(5)
N−Rh−N″	82.64(8)	N′−N−C(2)	108.19(10)
N−Rh−M	174.16(12)	C(2)−C(1)−C(2′)	105.8(2)
N−Rh−M″	91.54(11)	N−C(2)−C(1)	108.9(2)
M−Rh−M″	94.28(14)	N−C(2)−C(3)	121.9(2)
Rh−N−N′	114.41(4)	C(1)−C(2)−C(3)	129.2(2)
Rh−N−C(2)	134.68(12)		

[a] Primed atoms are related to the unprimed ones by the symmetry transformations $^1/_2 + y$, $-^1/_2 + x$, *z* (primed) and $^1/_2 - y$, $^1/_2 - x$, *z* (doubly primed). M represents the midpoint of the olefinic C(4)−C(5) bond.

(20) Shorter Rh−Rh separations have been observed in complexes with a Rh(μ-RPz)$_2$Rh framework as the result of redox processes generating direct metal−metal bonds; these are the cases of [CpRh(μ-Pz)]$_2$ (2.657(3) Å),[1f] [(CO)BrRh(μ-Pz)$_2$(μ-PPh$_2$C$_6$F$_4$)Rh(PPh$_2$C$_6$F$_4$Br)] (2.581(3) Å),[13a] and [{RhI(CO)}$_2$(μ-dppm)(μ-Pz)$_2$] (2.612(3) Å).[1d] Longer intermetallic separations have been reported in the rare related complexes with a chairlike conformation of the Rh(μ-RPz)$_2$Rh skeleton as in [{Cp*Rh(Pz)}$_2$(μ-Pz)$_2$] (4.103(1) Å; Oro, L. A.; Carmona, D.; Lamata, M. P.; Foces-Foces, C.; Cano, F. H. *Inorg. Chim. Acta* **1985**, *97*, 19) or [{Cp*RhCl}$_2$(μ-Pz)$_2$] (4.059(2) Å).[1f]

(21) Cremer, D.; Pople, J. A. *J. Am. Chem. Soc.* **1975**, *97*, 1354.

Table 3. Selected Bond Lengths (Å) and Angles (deg) for 4

Rh(1)···Rh(2)	3.8996(6)		
Rh(1)−N(1)	2.082(3)	Rh(2)−N(2)	2.084(3)
Rh(1)−N(3)	2.087(3)	Rh(2)−N(4)	2.081(3)
Rh(1)−C(10)	1.898(4)	Rh(2)−C(30)	1.892(5)
Rh(1)−C(20)	1.882(4)	Rh(2)−C(40)	1.881(5)
N(1)−N(2)	1.359(5)	N(3)−N(4)	1.366(5)
N(1)−C(1)	1.344(5)	N(3)−C(4)	1.335(5)
N(2)−C(3)	1.347(5)	N(4)−C(6)	1.349(5)
C(1)−C(2)	1.367(6)	C(4)−C(5)	1.385(7)
C(2)−C(3)	1.359(7)	C(5)−C(6)	1.371(7)
N(5)−C(10)	1.148(5)	N(5)−C(11)	1.440(5)
N(6)−C(20)	1.162(6)	N(6)−C(21)	1.455(6)
N(7)−C(30)	1.162(6)	N(7)−C(31)	1.439(6)
N(8)−C(40)	1.158(6)	N(8)−C(41)	1.431(6)
N(1)−Rh(1)−N(3)	91.57(13)	N(2)−Rh(2)−N(4)	91.33(13)
N(1)−Rh(1)−C(10)	91.0(2)	N(2)−Rh(2)−C(30)	178.0(2)
N(1)−Rh(1)−C(20)	173.1(2)	N(2)−Rh(2)−C(40)	91.6(2)
N(3)−Rh(1)−C(10)	174.8(2)	N(4)−Rh(2)−C(30)	90.0(2)
N(3)−Rh(1)−C(20)	91.4(2)	N(4)−Rh(2)−C(40)	173.7(2)
C(10)−Rh(1)−C(20)	85.6(2)	C(30)−Rh(2)−C(40)	86.9(2)
Rh(1)−N(1)−N(2)	127.8(3)	Rh(2)−N(2)−N(1)	127.2(2)
Rh(1)−N(1)−C(1)	124.7(3)	Rh(2)−N(2)−C(3)	125.7(3)
Rh(1)−N(3)−N(4)	126.9(2)	Rh(2)−N(4)−N(3)	127.8(2)
Rh(1)−N(3)−C(4)	125.3(3)	Rh(2)−N(4)−C(6)	124.9(3)
Rh(1)−C(10)−N(5)	176.0(4)	Rh(2)−C(30)−N(7)	179.0(4)
Rh(1)−C(20)−N(6)	174.6(4)	Rh(2)−C(40)−N(8)	176.4(4)
C(10)−N(5)−C(11)	174.0(5)	C(30)−N(7)−C(31)	171.4(5)
C(20)−N(6)−C(21)	169.3(5)	C(40)−N(8)−C(41)	171.9(5)

Table 4. Selected Bond Lengths (Å) and Angles (deg) for 8[a]

Rh(1)···Rh(2)	3.1553(11)		
Rh(1)−N(1)	2.073(6)	Rh(2)−N(2)	2.077(7)
Rh(1)−N(3)	2.075(8)	Rh(2)−N(4)	2.049(10)
Rh(1)−C(17)	2.129(8)	Rh(2)−C(7)	1.877(10)
Rh(1)−C(18)	2.135(9)	Rh(2)−C(8)	1.893(13)
Rh(1)−C(19)	2.142(9)	Rh(1)−M(1)	2.016(10)
Rh(1)−C(20)	2.097(9)	Rh(1)−M(2)	2.001(10)
N(1)−N(2)	1.355(9)	N(3)−N(4)	1.369(11)
N(1)−C(1)	1.327(10)	N(3)−C(4)	1.358(13)
N(2)−C(3)	1.332(10)	N(4)−C(6)	1.375(14)
C(1)−C(2)	1.381(13)	C(4)−C(5)	1.37(2)
C(2)−C(3)	1.402(13)	C(5)−C(6)	1.35(2)
N(5)−C(7)	1.162(11)	N(5)−C(9)	1.425(11)
N(6)−C(8)	1.145(13)	N(6)−C(10)	1.445(13)
C(17)−C(18)	1.384(13)	C(19)−C(20)	1.398(12)
N(1)−Rh(1)−N(3)	88.8(3)	N(2)−Rh(2)−N(4)	89.9(3)
N(1)−Rh(1)−M(1)	178.2(3)	N(2)−Rh(2)−C(7)	176.1(3)
N(1)−Rh(1)−M(2)	91.9(3)	N(2)−Rh(2)−C(8)	91.8(3)
N(3)−Rh(1)−M(1)	91.4(4)	N(4)−Rh(2)−C(7)	87.6(4)
N(3)−Rh(1)−M(2)	172.5(4)	N(4)−Rh(2)−C(8)	178.3(4)
M(1)−Rh(1)−M(2)	88.1(4)	C(7)−Rh(2)−C(8)	90.7(4)
Rh(1)−N(1)−N(2)	114.9(5)	Rh(2)−N(2)−N(1)	116.5(5)
Rh(1)−N(3)−N(4)	110.5(6)	Rh(2)−N(4)−N(3)	120.6(6)
Rh(1)−N(1)−C(1)	135.7(6)	Rh(2)−N(2)−C(3)	134.7(7)
Rh(1)−N(3)−C(4)	134.5(8)	Rh(2)−N(4)−C(6)	132.5(9)
C(7)−N(5)−C(9)	167.8(9)	Rh(2)−C(7)−N(5)	176.9(10)
C(8)−N(6)−C(10)	173.8(12)	Rh(2)−C(8)−N(6)	178.7(9)

[a] M(1) and M(2) represent the midpoints of the olefinic C(17)−C(18) and C(19)−C(20) bonds, respectively.

rhodium atoms. The Cremer and Pople puckering parameters for these complexes are listed in Table 6.[21] The relative folding of the structures, in terms of the dihedral angle between the two "Rh−N−N−Rh" bridging moieties (β angle) or between the two metal coordination planes (α angle), is closely associated with the intermetallic separation: longer intermetallic distances imply greater values of both dihedral angles (Table 6). Nevertheless, the α angle is more sensitive to the modifications in the metal−metal separations (range 67.48(6)−127.3(1)°), while the β angle changes to a lesser extent (92.95(3)−129.0(1)°). Interestingly, the

Table 5. Bond Lengths (Å) and Selected Angles (deg) for 9[a]

Rh···Rh′	3.5467(4)		
Rh−N(1)	2.065(3)	Rh−N(2)	2.058(2)
Rh−C(1)	1.854(4)	Rh−C(2)	1.859(3)
N(1)−N(1′)	1.364(5)	N(2)−N(2′)	1.356(4)
N(1)−C(3)	1.345(4)	N(2)−C(5)	1.349(3)
C(3)−C(4)	1.349(5)	C(5)−C(6)	1.368(4)
C(1)−O(1)	1.128(4)	C(2)−O(2)	1.129(4)
N(1)−Rh−N(2)	89.27(9)	Rh−N(1)−N(1′)	121.90(7)
N(1)−Rh−C(1)	178.82(12)	Rh−N(1)−C(3)	131.0(2)
N(1)−Rh−C(2)	91.48(14)	N(1′)−N(1)−C(3)	107.0(2)
N(2)−Rh−C(1)	89.56(12)	Rh−N(2)−N(2′)	122.16(6)
N(2)−Rh−C(2)	178.81(11)	Rh−N(2)−C(5)	130.1(2)
C(1)−Rh−C(2)	89.7(2)	N(2′)−N(2)−C(5)	107.4(2)
Rh−C(1)−O(1)	178.9(3)	N(1)−C(3)−C(4)	110.0(4)
Rh−C(2)−O(2)	179.3(3)	N(2)−C(5)−C(6)	110.2(3)

[a] Primed atoms are related to the unprimed ones by the symmetry transformation $x, 1/2 - y, z$.

Table 6. Geometrical Parameters of the Metallacycles[a]

	3	8	9	4
Rh···Rh, Å	3.0961(2)	3.1553(11)	3.5467(4)	3.8996(6)
α, deg	66.99(8)	72.0(2)	97.09(6)	127.32(11)
β, deg	92.90(4)	102.6(2)	111.95(8)	129.00(10)
Q, Å	1.776	1.346(6)	1.0855	0.822(2)
ϕ, deg	180.0	177.6(3)	180.0	−177.0(2)
θ, deg	90.0	92.9(3)	90.0	89.6(2)

[a] α is the dihedral angle between the coordination planes of the two metals; β is the dihedral angle between the two Rh−N−N−Rh planes; Q, ϕ, and θ are the Cremer and Pople parameters.

Rh−N distances observed in the four complexes are in a narrow range, 2.049(10)−2.087(3) Å, and compare well with the mean value obtained in Rh(I) square-planar complexes containing the rhodium−pyrazolate bonds (2.07(2) Å).

Within the molecular structure of **3** the ethylene molecules coordinate to the metals in a usual η^2-olefinic mode. The Rh−C bond distances (2.151(3) and 2.147(4) Å) are clearly in the upper limit of the range of values reported for related ethylene−rhodium complexes, indicating a weak interaction between the rhodium atoms and the olefins. Assuming the Chatt−Dewar scheme to describe the bonding of the ethylene ligand, the apparently weak Rh−olefin interaction is additionally supported by the C−C bond length (1.335(5) Å), which exhibits the smallest value reported so far for rhodium complexes,[22] shorter than those observed in tetracoordinate acetylacetonate derivatives such as [Rh(acac)-$(C_2H_4)_2$] (1.41(3) Å), [Rh(acac)$(C_2H_4)_2(C_2F_4)$] (average 1.41(2) Å),[23] and [Rh(1,3-ferrocenyl-acac)$(C_2H_4)_2$] (1.37-(1), 1.39(1) Å)[24] or in formally-pentacoordinate complexes of the general formulae [Rh(η^5-L)$(C_2H_4)_2$] (L =

(22) A search of rhodium-bonded ethylene molecules in the CSD database showed only one case with a statistically comparable C-C distance: 1.31(3) Å in [Rh(acac)$(C_2H_4)(CF_3C{\equiv}CCF_3)$] (Barlow, J. H.; Curl, M. G.; Russell, D. R.; Clark, G. R. *J. Organomet. Chem.* **1982**, *235*, 231). Unfortunately, the high error associated to this measurement reduces its reliability.

(23) Evans, J. A.; Russell, D. R. *J. Chem. Soc., Chem. Commun.* **1971**, 197.

(24) Cullen, W. R.; Rettig, S. J.; Wickenheiser, E. B. *J. Mol. Catal.* **1991**, *66*, 251.

(25) Marder, T. B.; Calabrese, J. C.; Roe, D. C.; Tulip, T. H. *Organometallics* **1987**, *6*, 2012.

(26) Rausch, M. D.; Spink, W. C.; Conway, B. G.; Rogers, R. D.; Atwood, J. L. *J. Organomet. Chem.* **1990**, *383*, 227.

(27) Kakkar, A. K.; Taylor, N. J.; Calabrese, J. C.; Nugent, W. A.; Roe, D. C.; Connaway, E. A.; Marder, T. B. *J. Chem. Soc., Chem. Commun.* **1989**, 990.

indenyl, 1.396 Å;[25] L = fulvalene, average 1.400(3) Å,[26] L = trimethylindenyl, 1.373(5) and 1.388(5) Å).[27] These bonding parameters are also in good agreement with the low activation energy measured in the spectroscopic experiments for the fluxionality (rotation) of the ethylene ligands (*vide infra*).

The four terminal $CNBu^t$ ligands present in **4** exhibit statistically identical Rh−C (mean 1.889(4) Å) and C−N (mean 1.157(4) Å) bond distances, and maintain a linear disposition around the coordinated carbon atom (mean Rh−C−N 176.5(9)°). These parameters compare well with those reported in the related A-frame rhodium(I) complex $[Rh_2(\mu\text{-dppm})_2(\mu\text{-}Me_2Pz)(CNBu^t)_2](PF_6)_2$ (Rh−C 1.920(10) Å, C−N 1.161(13) Å) where the isocyanide group is also *trans* disposed to a bridging pyrazolate.[28] Other closely related isocyanide-containing rhodium(I) complexes are the mononuclear $[Rh\{HB(3,5\text{-}Me_2Pz)_3\}(CNR)_2]$ (R = neopentyl, Rh−C 1.872(4) and 1.884(4), C−N 1.165(6) and 1.156(5) Å; R = $C_6H_3Me_2$, Rh−C 1.86(1) and 1.879(9) Å, C−N 1.17(1) and 1.16(1) Å) compounds,[29] in which two substituted *cis*-isocyanide ligands shared the central metal with two 3,5-dimethylpyrazolate ligands of the pyrazolylborate group. Interestingly, the bonding parameters observed for the isocyanide ligands in **8** (mean values Rh−C 1.883(8) Å, C−N 1.155(8) Å, Rh−C−N 177.9(9)°) do not differ significantly from those found in the tetraisocyanide derivative **4**.

The distances between the metal and the midpoints of the olefinic bonds in **8**, 2.016(10) and 2.001(10) Å, do not reflect any significant change in the bonding parameters of the cod molecule if compared with those reported in the closely related complexes $[Rh_2(\mu\text{-}Pz)_2(cod)_2]$ (average 2.020(12) Å)[30] or $[Rh_2(\mu\text{-}Me_2pz)_2(cod)_2]$ (average 2.016(2) Å)[31] where two terminal cod ligands are present. Analogously, the Rh−C bond distances involving the carbonyl ligands in **9** exhibit values, 1.854(4) and 1.859(3) Å, statistically identical to those described in the complex $[Rh_2(\mu\text{-}Me_2pz)_2(CO)_2]$ (range 1.848(5)−1.871(5) Å).[31]

The Fluxional Behavior of (Pyrazolato)rhodium Complexes. Ethylene Complexes. The variable temperature ^1H NMR spectra for the ethylene complexes **1** and **3** clearly reveal the occurrence of a fluxional process. They show well-resolved multiplets for the ethylenic protons at room temperature, interpretable as the AA′ and BB′ parts of a second-order AA′BB′X spin system. When the temperature is lowered, these two olefinic resonances coalesce into a single broad signal at δ *ca.* 3 ppm and split at 183 K in four multiplets as expected in the low-exchange region. For this behavior two motions leading to an AA′BB′X from an ABCDX spin system can be proposed, *(i)* the ethylene rotation around the coordinating bond which interconverts the *trans* ethylenic protons (A↔C)(B↔D), and *(ii)* an inversion of the boat conformation of the six-membered $Rh(N{-}N)_2Rh$ ring which interconverts the *cis* ethylenic protons (A↔D)(B↔C) (Figure 6). As the simultaneous occurrence of both intramolecular processes would lead to a single doublet in the spectrum (A_4X system), only one of them takes place in the range of temperatures studied (183−353 K).

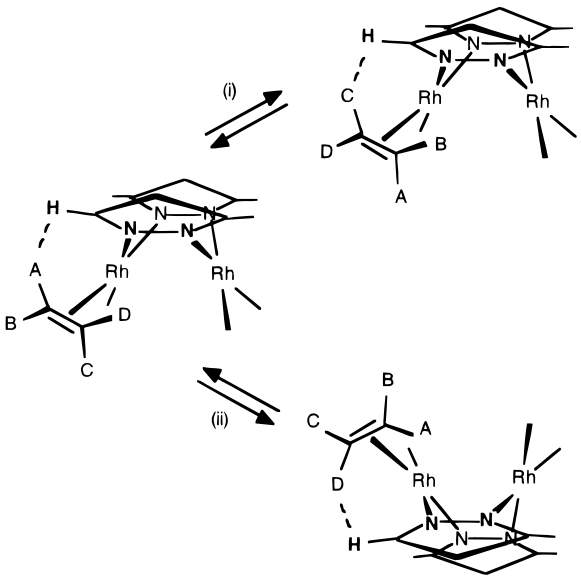

Figure 6. Possible motions for complexes **1**−**3**: (i) ethylene rotation; (ii) "$Rh(N{-}N)_2Rh$" ring inversion. The dotted lines show the close proximity between one olefinic and one Pz protons.

The dynamic behavior of **1** is successfully simulated by assuming the chemical exchange of the *trans* olefinic protons (A↔C)(B↔D) exclusively. No detectable broadening of the ethylene resonances but only an appreciable decomposition of **1** is observed when the temperature is raised to 353 K. Therefore, rotation of ethylene is the only process which appears to take place. This implies that there is no facile inversion of the central $Rh(N{-}N)_2Rh$ ring on the NMR time scale for these complexes. The same process should thus occur for **3**, although a similar simulation was not performed because the static spectrum could not be obtained. A plot of ln(*k*) *vs* 1/*T* for **1** is linear and gives an activation energy of 10.0 kcal·mol^{-1} for the rotation of the ethylene ligands. From the plot of ln(k/T) *vs* 1/*T*, the values $\Delta H^{\neq} = 9.50$ kcal·mol^{-1} and $\Delta S^{\neq} = -0.65$ eu are found. These values are smaller than those found for the mono and dinuclear complexes $[Rh(C_5H_5)(C_2H_4)_2]$,[32] $[Rh(acac)(C_2H_4)_2]$,[33] and $[Rh_2(\eta^5\text{-}\eta^5\text{-fulvalene})(C_2H_4)_4]$[26] and slightly larger than those for the indenyl complexes $[Rh(\eta^5\text{-L})(C_2H_4)_2]$.[27] The origin of this low activation energy value is associated, most probably, with the weak $Rh{-}C_2H_4$ bond also detected by the X-ray diffraction study of the related complex **3**.

Diolefin Complexes. Figure 7 shows the pyrazolate and olefinic regions of selected ^1H and $^{13}C\{^1H\}$ NMR spectra from a mixture of $[\{Rh(\mu\text{-Pz})(CNBu^t)_2\}_2]$ (**4**), $[\{Rh(\mu\text{-Pz})(cod)\}_2]$ (**7**) and $[(cod)Rh(\mu\text{-Pz})_2Rh(CNBu^t)_2]$ (**8**) in benzene-d_6. The spectra demonstrate both compounds (**7** and **8**) to be rigid on the NMR time scale at 283 K. When the temperature increases compound **8** becomes fluxional: the two resonances (labeled with an asterisk) produced by the olefinic protons and carbons inside and outside of the pocket of **8** transform into

(28) Tortorelli, L. J.; Woods C.; Campana C. F. *Acta Crystallogr.* **1992**, *C48*, 1311.
(29) Jones, W. D.; Hessell, E. T. *Inorg. Chem.* **1991**, *30*, 778.
(30) Beveridge, K. A.; Bushnell, G. W.; Stobart, S. R.; Atwood, J. L.; Zaworotko, M. J. *Organometallics* **1983**, *2*, 1447.
(31) Louie, B. M.; Rettig, S. J.; Storr, A.; Trotter, J. *Can. J. Chem.* **1984**, *62*, 1057.
(32) Cramer, R.; Kline, J. B.; Roberts, J. D. *J. Am. Chem. Soc.* **1969**, *91*, 2519.
(33) Herberhold, M.; Kreiter, C. G.; Wiedersatz, G. O. *J. Organomet. Chem.* **1976**, *120*, 103.

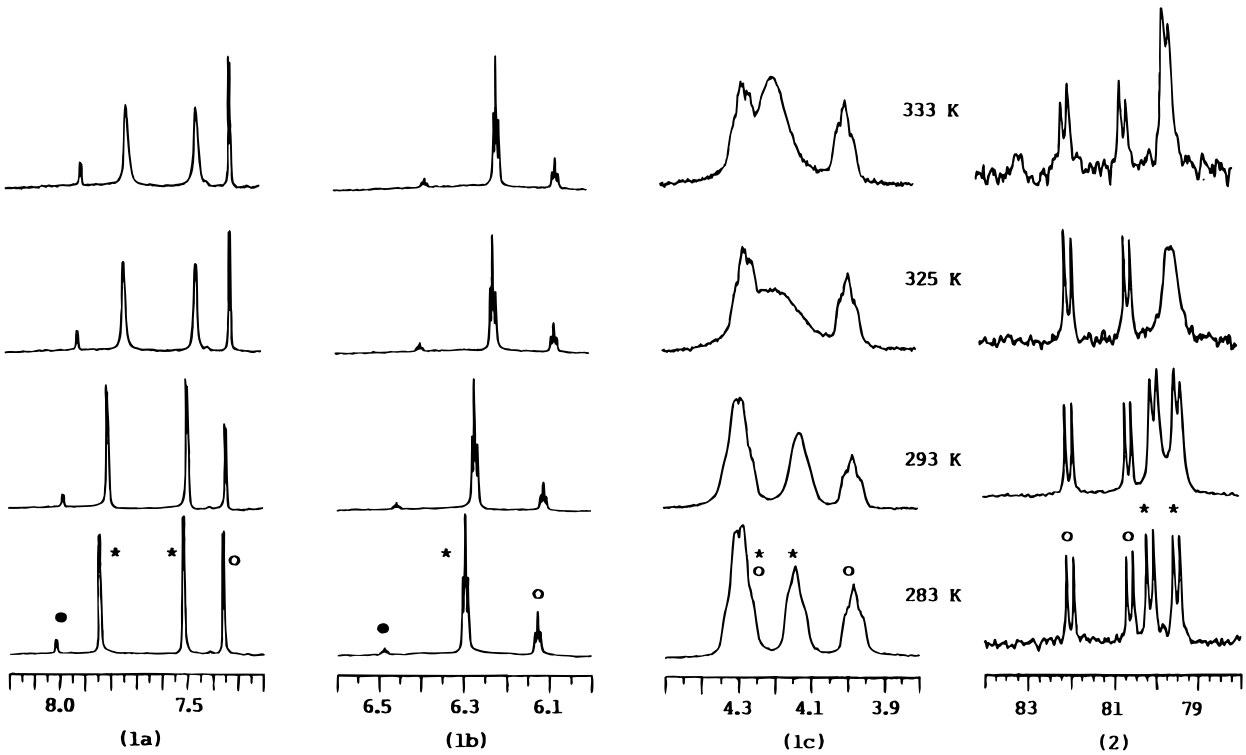

Figure 7. Selected regions of variable temperature ^1H (1a−c) and $^{13}C\{^1H\}$ (2) NMR spectra for a mixture of complexes **4** (●), **7** (○) and **8** (*)

single broadened lines at 333 K. It is important to note that at this temperature the olefinic carbons remain coupled to rhodium. Therefore, the observed process does not involve dissociation of the cod ligand. The second spectroscopic feature of compound **8** consists of the line broadening effect observed for the H^3 and H^5 resonances above 325 K. These become a broadened singlet at 373 K in toluene-d_8 due to a H^3-H^5 positional exchange. It follows from the above spectra that two different fluxional processes take place in complex **8**. Both processes seem to be intramolecular as a 10-fold variation of concentration of the investigated solutions gives the same temperature behavior of complex **8**. In accord with these results, two different sets of activation parameters have been obtained from the lineshape analysis of the ^1H and $^{13}C\{^1H\}$ NMR spectra carried out by the use of DNMR6 program: $\Delta H^{\neq} = 15.0$ kcal·mol^{-1}, $\Delta S^{\neq} = -1.7$ eu and $\Delta H^{\neq} = 19.7$ kcal·mol^{-1}, $\Delta S^{\neq} = 4.8$ eu for the "olefinic" and H^3-H^5 positional exchanges, respectively. It should be noted that the very small $\Delta S^{\neq}$ values are in agreement with the intramolecular character of both processes.

Discussion

Almost all dinuclear complexes containing two pyrazolate bridges have a boat conformation for the six-membered ring "$M(N-N)_2M$" in the solid state. A possible fluxional behavior could involve a boat−boat inversion previously suggested[1f,4,15c] for these dinuclear complexes but has not been observed so far. Thus, studies on the dynamic behavior of [{Rh(μ-Pz)(cod)}$_2$] detected a slight line broadening suggesting a high-energy process. The fluxionality found for **1**−**3** and **8** provides a good opportunity to obtain a better understanding of the dynamic behavior of dinuclear rhodium pyrazolato compounds.

The results of the variable temperature study on the ethylene complexes **1**−**3** clearly show that rotation of ethylene is the only possible motion detected between 180 and 353 K. The absence of the boat−boat inversion in these dinuclear pyrazolato complexes and the apparently high-energy process of those containing 1,5-cyclooctadiene as ancillary ligands, such as **7**, raises some speculation about its origin. The boat−boat inversion should involve an opening of the the dihedral angle (α) defined by the square-planar environments of the rhodium atoms. However, this feasible motion should be restricted because of the rigidity of the aromatic bridging ligands, and it cannot be sequential like in cyclohexane but concerted, as described for 5,10-dihydroanthracene or cyclooctatetraene. Thus, as the α angle increases the boat conformation of the six-membered "$Rh(N-N)_2Rh$" ring becomes closer to a planar conformation.

The study of this potential movement with the help of Walsh diagrams varying α between 60 and 180° for the complexes [{Rh(μ-RPz)L_2}$_2$] (RPz = Me_2Pz, L_2 = $(C_2H_4)_2$ (**3**), cod, $(CO)_2$; RPz = Pz, L_2 = cod (**7**), $(CO)_2$ (**9**), $(CNBu^t)_2$ (**4**)) using their crystallographic data reveals that it is affected by electronic and steric factors. The EHMO[34] computational method was used in this study, but because of its well-known shortcomings, arguments based in the absolute energies and charges were avoided. Therefore, we have tried to interpret the relative differences in these values for the compounds investigated from a qualitative approach. From an electronic point of view, a close proximity of the metallic centres is hindered by the repulsive interaction between the two filled d_{z^2} and, to a lesser extent, by the d_{xz} and d_{yz} metal orbitals. On the other hand, the opening of

(34) Hoffmann, R. *J. Chem. Phys.* **1963**, *39*, 1397. Hoffman, R.; Lipscomb, W. N. *J. Chem. Phys.* **1962**, *36*, 2179; 2872.

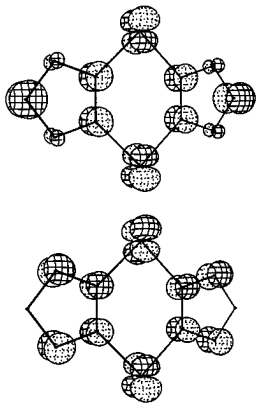

Figure 8. CACAO drawings showing the repulsive interaction between the metallic d_{xz} orbitals and the pyrazolate e_1'' set.

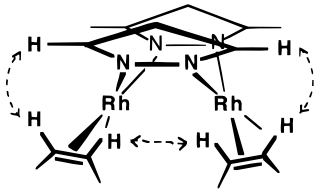

Figure 9. Nonbonding H−H interactions between the 3- and 5-pyrazolate and olefinic protons outside and inside the pocket of the complexes.

the α angle toward a planar conformation is limited by the interaction between the occupied metallic d_{xz}, d_{yz} orbitals and the e_1'' orbital sets of the pyrazolate ligands (Figure 8), reaching a maximum at α = 180°. From a steric point of view, molecular models for **1** and **7** (based on crystallographic bonding distances and angles) show that as the boat conformation approaches the planar conformation, four repulsive nonbonding hydrogen−hydrogen interactions appear between the protons of ancillary olefin ligands and those in the 3- and the 5-positions of the pyrazolate bridging ligands (Figure 9). Furthermore, if there are methyl groups in these positions such as in the complexes [{Rh(μ-Me_2Pz)L_2}$_2$] (L_2 = $(C_2H_4)_2$ (**3**), cod (**10**)) the steric hindrance is such that the planar conformation cannot be reached simply for reasons based on steric grounds. Therefore, it does not seem surprising that complexes with 3,5-Me_2Pz bridging ligands and olefinic ancillary ligands show no evidence for a boat−boat inversion.

For the complexes with unsubstituted pyrazolate bridging ligands with olefinic ancillary ligands [{Rh(μ-Pz)L_2}$_2$] (L_2 = $(C_2H_4)_2$ (**1**), cod (**7**)) the calculated energy values of this barrier are 3.48 and 3.13 eV (80.2 and 72.1 kcal·mol^{-1}), respectively. In contrast, for the complexes [{Rh(μ-Pz)L_2}$_2$] (L = CO (**9**), $CNBu^t$ (**4**)), without the steric hindrance above mentioned, values of 1.25 and 1.40 eV (28.7 and 32.1 kcal·mol^{-1}) respectively are obtained. This is consistent with the lack of the boat−boat inversion for the olefinic compounds, but it shows that it could be operative in complexes **4** and **9**. Unfortunately, the high symmetry of these complexes, which makes the protons H^3 and H^5 indistinguishable, prevents detection by NMR measurements. However, the complex [(cod)Rh(μ-Pz)$_2$Rh($CNBu^t$)$_2$] (**8**) provides a rare opportunity to observe the occurrence of this or any other similar motion. The energy barrier calculated for the boat−boat inversion for this complex **8** is 2.29 eV (52.7 kcal·mol^{-1}), nearly the mean value of those calculated for **4** and **7**, possibly because only two repulsive nonbonding hydrogen−hydrogen interactions should be present in the planar conformation.

From the two fluxional processes detected for **8**, the former process appears to be a result of the rotation around the axis defined by the metal−olefin bond or around the bisectrix of the angle centred on the rhodium and the two olefinic bonds. The first possibility is unrealistic due to the rigidity of the cod ligand. The second interpretation would also seems unlikely because, in such case, a tetrahedral rhodium transition state would result. A theoretical calculation for the latter process gives a value of 3.09 eV (71.3 kcal·mol^{-1}) for the energy barrier, while 2.29 eV (52.7 kcal·mol^{-1}) is obtained for an alternative boat−boat inversion. Therefore, we propose the lowest energy process, i.e. the boat−boat inversion (Figure 10), as the most probable for the fluxional behavior of the inside−outside protons and carbons.

In addition, we have observed environment effects on the "olefin" fluxional motion which have no influence on the H^3−H^5 exchange; in other words, the two processes are independent. In donor solvents such as acetone-d_6 the value of the exchange rate for the "olefin" motion in **8** is almost double, 28.1 s^{-1}, compared with 17.4 s^{-1} in benzene-d_6 or toluene-d_8 at the same temperature (293 K). A similar increase of the exchange rate is observed upon addition of an small amounts of pyrazole to a benzene-d_6 solution (29.4 s^{-1} at 293 K). Furthermore, addition of pyrazole to a acetone-d_6 solution leads to a 3-fold increase of the rate constant (51.0 s^{-1} at 293 K). It should be noted that there is no exchange between the free pyrazole and coordinated pyrazolate on the NMR time scale. In addition, there is no difference of the bandwidth at half-height for the pyrazolate resonances between the spectra of **8** at 333K in benzene-d_6 and in acetone-d_6 even if pyrazole is added. These surprising results suggest an alternative pathway for the "olefin" motion associated with the presence of donor species in the solution which again has no relation to the H^3−H^5 exchange. Moreover, the addition of pyrazole to the benzene-d_6 solutions of [{Rh(μ-Pz)(cod)}$_2$] (**7**) and [{Rh(μ-Me_2Pz)(cod)}$_2$] (**10**), which show static ^{1}H NMR spectra in pure benzene-d_6, accelerates the exchange between the inside−outside protons (k = 14.1 s^{-1} for **7** at 328 K). As the boat−boat inversion has been considered impossible for [{Rh(μ-Me_2Pz)(cod)}$_2$], an alternative, solvent-assisted associative pathway, should involve a five-coordinate intermediate, commonly observed in substitution reactions of square planar 16-e complexes,[35] where a Berry pseudorotation of the cod ligand would account for this exchange (Figure 11).

The second dynamic process for **8**, which involves the H^3−H^5 exchange, could appear as a rotation of the pyrazolate bridging ligands around the axis containing the C^4−H^4 bond. The NMR data imply that complete dissociation of pyrazolate does not occur because it is not influenced by the presence of free pyrazole, although the breaking of at least one Rh−N bond is necessary to explain this exchange. This breaking would lead to a 14-electron Rh species, as proposed for bis(pyrazol-1-yl)palladium complexes.[36] In the case of **8**, the breaking

(35) Atwood, J. D. *Inorganic and Organometallic Reaction Mechanisms*; Brooks/Cole Publishing Company: Monterey, CA, 1985.

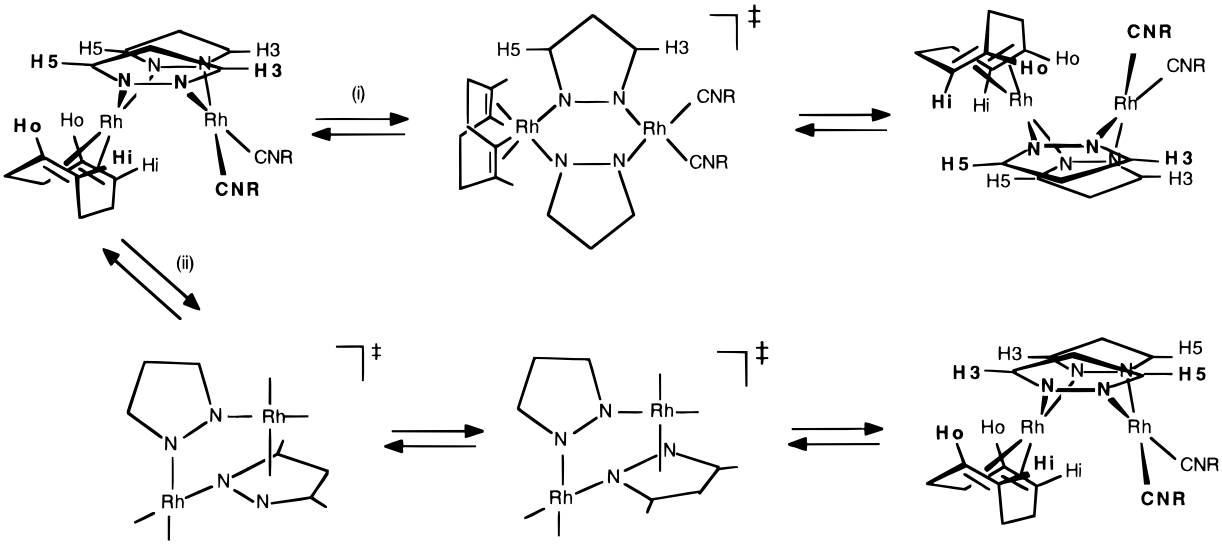

Figure 10. Proposed motions for complex [(cod)Rh(μ-Pz)$_2$Rh(CNBu^t)$_2$] (**8**): (i) "Rh(N−N)$_2$Rh" ring inversion; (ii) σ-1,2-metallotropic shift.

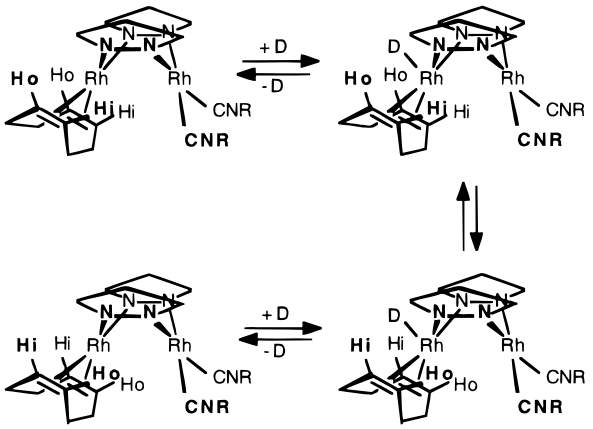

Figure 11. Proposed fluxionality of the complex [(cod)-Rh(μ-Pz)$_2$Rh(CNBu^t)$_2$] (**8**) in the presence of donors (D).

of a Rh−N bond is necessary but the presence of a 14-electron Rh complex is not probable due to the absence of donor medium effects on the exchange. Molecular models show that after the Rh−N bond breaking, the aromatic ring of the resulting monocoordinated pyrazolate ligand lies in close proximity and in the appropriate orientation to interact in a π-fashion with the 14-electron Rh species. At this stage, ring slippage of the π-coordinated pyrazolate, exchanging the nitrogen directly bonded to the rhodium, followed by re-formation of the Rh−N bond would produce the observed H^3−H^5 exchange (Figure 10). This motion could also be described as a σ-1,2-metallotropic shift. In accordance with this proposal, previous haptotropic shifts observed in square-planar mononuclear complexes with N-donor ligands, having energy barriers ($\Delta G^{\neq 298}$ = 18.3 kcal·mol^{-1}) similar to that found for complex **8**, have been reasonably explained in terms of a sliding mechanism.[37] As the ring slippage requires the breaking of one Rh−N bond, its energy barrier should be closely related to the Rh−N bond energy. This suggests therefore, that in similar pyrazolato complexes the sliding process should also occur. Nevertheless, it would only be detectable if the 3- and 5-positions of the pyrazolate bridging ligands are inequivalent. Support for this hypothesis comes from a ^{1}H NMR variable-temperature study on the complex [{Rh(μ-MePz)(cod)}$_2$] (**11**) which exists in solution as a mixture of the HH and HT isomers. In these isomers, the steric hindrance between the methylpyrazolate groups and the olefinic protons of the cod ligands prevents the boat−boat inversion; however, the sliding mechanism alows an interconversion between the HH and the HT isomers, which is indeed observed. At 22 °C in toluene-d_8 both isomers are present in a 1:1.7 molar ratio. On increasing the temperature, a neat broadening of the resonances corresponding to both isomers is observed, and the coalescence occurs at 85 °C. Further confirmation of this interconversion comes from the cross peaks observed in the NOESY spectrum at room temperature.

Having demonstrated the feasibility of this exchange mechanism, there are reasons to suppose that a similar motion involving the breaking of the Rh−N bond also takes place in symmetrical pyrazolato complexes, although it cannot be detected.

In addition, compound **8** transforms into **4** and **7**, but the chemical equilibrium is not observable on the NMR time scale. This is a second order reaction, and hence in the transition state two molecules of **8** collides to give **4** and **7** and *vice versa*. The value of $\Delta G^{\neq 298}$ for the chemical reaction (24.0 kcal·mol^{-1}) higher than for the high energy fluxional process (18.3 kcal·mol^{-1}) suggests that the effective collisions probably involve one dinuclear species with a broken Rh−N bond. Thus, dinuclear rhodium species seems to be responsible for the redistribution reactions, an observation consistent with the resistance of the dinuclear (pyrazolato)rhodium complexes toward fragmentation; *e.g.*, no reaction was observed when the complex [{Rh(μ-Pz)(cod)}$_2$] was refluxed with PPh$_3$.[1a]

The Intermetallic Distance in (Pyrazolato)-rhodium Complexes. Another interesting feature of the pyrazolate bridging ligand is the flexibility the group provides for the corresponding dinuclear complexes in terms of the metal−metal separation. This flexibility

(36) Jalon, F. A.; Manzano, B. R.; Otero, A.; Rodríguez-Pérez, M. C. *J. Organomet. Chem.* **1995**, *494*, 179.
(37) Alvarez, S.; Bermejo, M. J.; Vinaixa, J. *J. Am. Chem. Soc.* **1987**, *109*, 5316.
(38) Schumann, H.; Hemling, H.; Ravindar, V.; Badrieh, Y.; Blum, J. *J. Organomet. Chem.* **1994**, *469*, 213.

Table 7. Rh···Rh Distances (Å) in Compounds of the Type [{Rh(μ-pz)(L)(L′)}$_2$]

Pz	L	L′	Rh···Rh	ref	complex
Me_2Pz	$(C_2H_4)_2$		3.0961(2)	this work	**3**
Me_2Pz	(cod)		3.1538(3)	31	**10**
Me_2Pz	CS	PPh_3	3.220	1b	
Me_2Pz	$(CO)_2$		3.262(4)	31	
Pz	(cod)		3.267(2)	30	**7**
Me_2Pz	CO	$PRPh_2$[a]	3.479(1)	38	
Pz	CO	$P(OPh)_3$	3.568	1a	
Pz	$(CO)_2$		3.5467(4)	this work	**9**
Pz	$(CNBu^t)_2$		3.8996(6)	this work	**4**

[a] R = 2-formylphenyl.

is associated with the opening of the dihedral α angle which, in turn, is closely related to the intermetallic distance. For example, the steric hindrance that appears to exist for the boat−boat inversion movement in the complexes [{Rh(μ-Me_2Pz)(L_2)}$_2$] (L_2 = $(C_2H_4)_2$ (**3**), cod (**10**)) implies that these molecules are forced to show relatively small dihedral angles α and, in consequence, short Rh−Rh distances. On steric grounds, larger intermetallic distances could be expected for analogous complexes containing sterically undemanding bridging (Pz) and/or terminal (CO, $CNBu^t$) ligands such as [{Rh(μ-Pz)($CNBu^t$)$_2$}$_2$].

Table 7 shows the reported Rh···Rh distances in complexes of the type [{Rh(μ-pz)(L)(L′)}$_2$]. These distances seem to result from a compromise between electronic and steric factors (see above). Systematically, shorter distances are observed for complexes with 3,5-Me_2Pz, compared with their unsubstituted counterparts, with identical ancillary ligands. Hence the steric factors involving the substituents of the pyrazolates determine the intermetallic separation and seem to outweigh the electronic effects in the region of *short intermetallic distances*. A similar idea for the related iridium complexes was proposed by Stobart for [{Ir(μ-R_2Pz)(cod)}$_2$] (R = Me, CF_3)[30] and by Storr for [{Ir(μ-R_2Pz)$(CO)_2$}$_2$] (R = H, Me).[39] In addition, the steric crowding in the pocket of the complexes also plays an important role concerning the intermetallic separation. Thus, for both series (the Me_2Pz and the Pz complexes), the intermetallic distance increases in going from the cod complex to the carbonyl complex, where there is no steric crowding. The shorter distance found for the ethylene complex **3** relative to that of the analogous cyclooctadiene complex **10** should be attributed to a better accommodation of the ethylene ligands compared with the rigidity imposed by the cod chelating cycle.

In the other extreme, the complex [{Rh(μ-Pz)($CNBu^t$)$_2$}$_2$] (**4**) has the largest distance found in d^8−d^8 rhodium or iridium dinuclear pyrazolato compounds. In this complex, the absence of substituents in the 3,5-positions of the pyrazolate bridging ligands together with the small cone angle of the ancillary ligands should lead to a long metal−metal distance. However, If we compare the intermetallic distances of [{Rh(μ-Pz)($CNBu^t$)$_2$}$_2$] (**4**) and [{Rh(μ-Pz)$(CO)_2$}$_2$] (**9**) the difference of *ca.* 0.4 Å cannot only be explained on steric grounds because the CO and $CNBu^t$ ligands show approximately the same steric hindrance with the pyrazolate bridging ligands. However, it is important to note that CO and $CNBu^t$ ligands show different electronic characteristics. $CNBu^t$ is a good σ-donor while the CO ligand is a good π-acceptor. According to this, a calculation of the Mulliken charge on the rhodium atoms of both compounds reveals that in **4** the rhodium atoms have a partial negative charge of −0.12 while in **9** it is +0.27. This depopulation, in **4** relative to that in **9**, fundamentally affects the HOMO orbital, mainly an out of phase combination of rhodium d_{z^2} orbitals,[40] and consequently allows a decrease in the intermetallic distance in *ca.* 0.4 Å. Therefore, the influence of the electronic effects becomes dominant in the *large intermetallic distance* region, where no significant steric effects are present.

Although most of the the known examples of symmetrical dinuclear pyrazolato complexes appear to be consistent with the above, the intermetallic distance of the complex [(cod)Rh(μ-$Pz)_2$Rh($CNBu^t$)$_2$] (**8**) is 3.1551(12) Å, shorter than that even for complex **7**. This apparently surprising result would appear to be in disagreement with our findings. In other words, from an electronic point of view, this complex can be envisaged as made from the halves of the complexes [{Rh(μ-Pz)(cod)}$_2$] and [{Rh(μ-Pz)($CNBu^t$)$_2$}$_2$] where a calculation of the Mulliken charge on both rhodium atoms in **8** gives a value of +0.35 for the Rh(cod) and −0.12 for the Rh($CNBu^t$)$_2$ moiety, values similar to those found for **7** (+0.31) and **4** (−0.12). In such case, an intermetallic distance of *ca.* 3.5 Å should be expected. However, the reason for the short Rh−Rh metal distance in **8** relative to that in **7** can be basically attributed to steric effects. A formal substitution of one cod ligand in **7** by two $CNBu^t$ groups removes the steric hindrance inside of the pocket of the complex, and hence the $H^{3,5}$(pyrazolate) and the $H^{outside}$(cod) hydrogens are allowed to become further appart. Thus, the metal atoms are obliged to move closer. Indeed, this effect is clearly observed by comparison of the crystal structures of the complexes **7** and **8**, where the separation between the pyrazolate $H^{3,5}$ and the cod olefinic hydrogens outside of the pocket is 2.099 Å in **7** while in **8** the average separation is 2.50 Å. In consequence, steric effects have a strong influence on the intermetallic distance in rhodium(I)−pyrazolato complexes as discussed previously.

Concluding Remarks

The synthesis of the mixed-ligand dinuclear complex [(cod)Rh(μ-$Pz)_2$Rh($CNBu^t$)$_2$] described herein is based on a ligand redistribution reaction between the symmetrical complexes [{Rh(μ-Pz)(cod)}$_2$] and [{Rh(μ-Pz)($CNBu^t$)$_2$}$_2$]. Kinetic studies carried out on the equilibrium show that the reaction follows a second-order rate, and it is associated with the breaking of at least one Rh−N bond. Hence, dinuclear complexes are the active species in this redistribution reaction, and therefore no fragmentation into mononuclear complexes occurs, in accordance with the remarkable stability of the "Rh(μ-$Pz)_2$Rh" framework. In addition, the complex [(cod)Rh(μ-$Pz)_2$Rh($CNBu^t$)$_2$] undergoes two independent fluxional processes. The low-energy process is believed to come from a ring inversion of the six-membered "Rh(μ-pz)$_2$Rh" metallacycle. Such a movement, suggested previously and very interesting for mechanistic propos-

(39) Nussbaum, S.; Rettig, S. J.; Storr, A.; Trotter, J. *Can. J. Chem.* **1985**, *63*, 692.

(40) Boyd, D. C.; Connelly, N. G.; García Herbosa, G.; Hill, M. G.; Mann, K. R.; Mealli, C.; Orpen, A. G.; Richardson, K. E.; Rieger, P. H. *Inorg. Chem.* **1994**, *33*, 960.

als, may be restricted by the ancillary ligands and the substituents on the pyrazolate rings in other bis(μ-pyrazolato) complexes. Donor species in the medium can lead to a fluxional behavior in bis(μ-pyrazolato) complexes with similar results, even where the ring inversion cannot take place by steric reasons. The high-energy process involves the breaking of a Rh−N bond followed by a sliding of one of the pyrazolate ligands or a σ-1,2-metallotropic shift, which should be the starting point for the above-mentioned redistribution reaction. Finally, the intermetallic distance in dinuclear pyrazolato complexes results from a compromise of steric and electronic factors. The steric crowding inside of the pocket of the complex and the electronic repulsion between the d_{z^2} metal orbitals operate to keep the metals separated, while a close contact between the rhodium atoms is favored by the electronic repulsion between the d_{xz} and d_{yz} metallic orbitals and the e_1'' of the pyrazolate bridging ligands and by repulsions between the substituents on the 3- and 5-positions of the pyrazolate ligands and the ancillary ligands. Apparently, the steric effects fundamentaly control the intermetallic distances, specially in the region of short Rh···Rh separations, while the electronic effects show their relevance in the long intermetallic distance region, where no significant steric influence is operational.

Appendix

Calculations of the extended Hückel type were carried out using a modified version of the Wolfsberg−Helmholz formula.[41] The geometrical parameters of the compounds investigated were as close as possible to the reported crystal structures. Atomic parameters used were those of Alvarez,[42] and the calculations and drawings were made with the program CACAO.[43]

Acknowledgment. We wish to thank DGICYT (Projects PB92 86-C02-02 and PB94-1186) and CICYT and Generalitat de Catalunya (Project QFN92-4311) for financial support. We also thank Iberdrola Company for an Iberdrola Visiting-Professorship to V.I.B.

Supporting Information Available: Crystal data and structure refinement (Tables S1 (**3**), S7 (**4**), S13 (**8**), and S19 (**9**)), atomic coordinates (Tables S2 (**3**), S8 (**4**), S14 (**8**), and S20 (**9**)), anisotropic displacement parameters (Tables S3 (**3**), S9 (**4**), S15 (**8**), and S21 (**9**)), all bond distances and angles (Tables S4 (**3**), S10 (**4**), S16 (**8**), and S22 (**9**)), least-squares planes (Tables S5 (**3**), S11 (**4**), S17 (**8**), and S23 (**9**)), and intermolecular contacts (Tables S6 (**3**), S12 (**4**), S18 (**8**), and S24 (**9**)) (66 pages). Ordering information is given on any current masthead page.

OM960005Y

(41) Ammeter, J. H.; Bürgi, H. B.; Thibeault, J. C.; Hoffmann, R. *J. Am. Chem. Soc.* **1978**, *100*, 3686.
(42) Alvarez, S. *Table of Parameters for Extended Hückel Calculations*; Departamento de Química Inorgánica, Universidad de Barcelona: Barcelona, Spain, 1989.
(43) Mealli, C.; Proserpio, D. M. *J. Chem. Educ.* **1990**, *67*, 399.